Algorithm Theoretical Basis Document

EOS/AMSR-E LEVEL-2 RAINFALL

Christian Kummerow, CSU

Ralph Ferraro, NOAA/NESDIS

July 2012

The AMSR-E Level 2 rainfall algorithm is rooted in a Bayesian retrieval scheme over oceans and a regression of scattering signals to surface rainfall over land (Wilheit et al. 2003; Wang et al. 2009; Gopolan et al. 2010). The ocean retrieval relies primarily on the emission signal from the rain drops themselves while the land retrieval relies solely on the scattering of high frequency (e.g., 89 GHz) radiation from precipitation sized-ice particles at and above the freezing level. The two approaches are needed due to the vastly different surface emissivities and the resulting differences in the sensor information content over ocean and land, respectively. In order to build a consistent algorithm framework, prior to the launch of the Aqua satellite, the land portion of the algorithm was converted from its original regression form (i.e., Grody 1991 and updated by Ferraro 1997) to a Bayesian framework, but in such a fashion as to currently reproduce the original regression equations (McCollum et al. 2003). Typical reflectivities for ocean and land conditions are shown in Fig. 1. The low reflectivity (large emissivity) over land limits the use of emission signals of the precipitation and forces the land algorithm to exploit only the scattering signals.

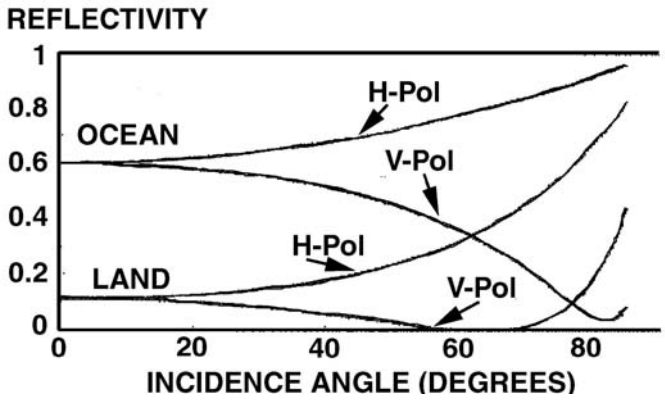

Figure 1: Reflectivity of typical ocean and land surfaces as a function of incidence angle for horizontal and vertical polarizations.

In an atmosphere that absorbs and/or scatters microwave radiation, the radiance is governed by the Equation of Radiative Transfer (RTE) (Chandrashekar 1960) which may be organized as:

$$\frac{dR(\theta,\phi)}{ds} = A + S \tag{1}$$

where: $A = \gamma_{abs}\left\{B(\lambda,T) - R(\theta,\phi)\right\}$, $S = \gamma_{sca}\left\{\iint P(\theta,\phi;\theta',\phi')R(\theta,\phi')d\Omega' - R(\theta,\phi)\right\}$, $R(\theta,\phi)$ is the radiance in the direction specified by the polar angles θ and ϕ, s is distance in the θ, ϕ direction, γ_{abs} is the absorption coefficient, and γ_{sca} is the scattering coefficient. $P(\theta, \phi, \theta', \phi')$ is the phase function that describes the probability of scattering from a direction specified by θ', ϕ' to a direction θ, ϕ and is normalized such that:

$$\int P(\theta,\phi;\theta',\phi')d\Omega' = \int P(\theta,\phi;\theta',\phi')d\Omega = 1\,. \tag{2}$$

Figure 2 shows the results of computations based on this model for frequencies of 6.9, 10.7, 18.7, 36.6 and 89.0 GHz viewing directly at the 54° incidence angle of the AMSR- E. An ocean background is assumed. The computations were carried out for several different freezing levels as indicated in the figure. While both horizontal and vertical polarizations are computed, only horizontal polarizations are shown in order to keep the figures legible. Note that at all frequencies, the brightness temperature increases towards a maximum and then drops off as rainfall rates increase even further. The key differences between the frequencies are the range of rainfall rates for which the curve increases (emission region) and the range for which the curves decrease (scattering region). Lower frequencies (e.g., 6.9-18 GHz) tend to increase through much of the rainfall range, thus, making them suitable for emission type schemes. Higher frequencies saturate rather quickly and decrease (scattering region) for much of the rainfall range. If these curves were shown over land, all curves would start at approximately 280 K due to high surface emission—showing little change from emission but the same general scattering trend. As such, the precipitation retrieval over oceans exploits both the emission and scattering signal while the land algorithm is confined to scattering signals alone.

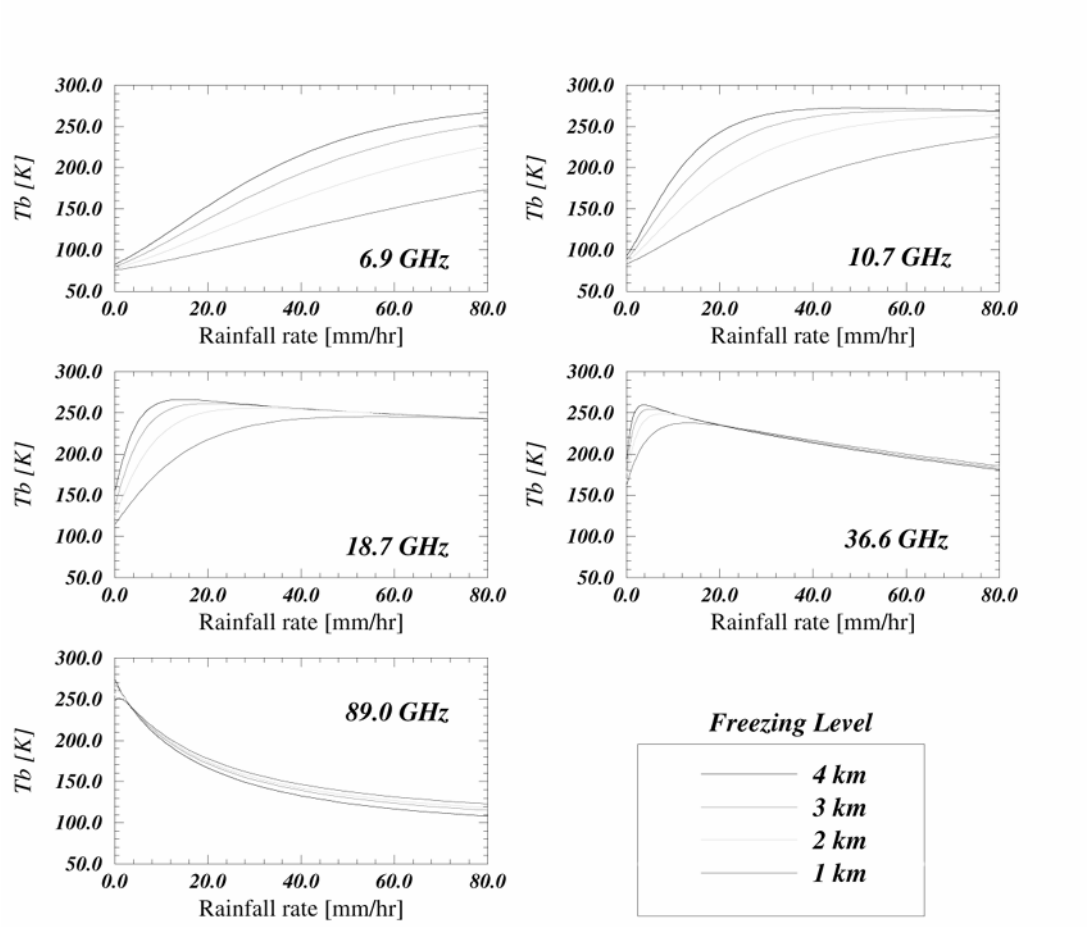

Figure 2: Computed brightness temperatures as a function of rainfall rate for selected AMSR-E frequencies

Instantaneous Ocean Rainfall

Radiative transfer calculations can be used to determine a brightness temperature, TB, given a temperature, water vapor and hydrometeor profile. An example of such a computation through the cloud structure assumed by Wilheit et al. (1977) is shown in Fig. 2. An inversion procedure, however, is needed to find a rainfall rate, R, given a brightness temperature, TB. At first glance, one might be tempted to simply invert the curves shown in Fig. 2, particularly since the double valued nature of the relations is easily resolved by a combination of two or more channels. Unfortunately, the relations derived in that example were applicable only to the 'average' cloud structure assumed in

that study. Since TBs are sensitive to the vertical structure of precipitation, the vertical structure cannot be ignored when instantaneous retrievals (Level 2 products) are sought. The sensitivity to the assumed profile gets larger as the frequency increases and the scattering in the upper layers of the cloud begin to play a larger role. Thus, one is left with a somewhat more complicated problem of finding the hydrometeor profile, R, given a set of TB*s* represented by the vector **TB**. The objective of the instantaneous rainfall algorithm over ocean is to find this profile R.

While the vertical structure of precipitation is extremely important in determining upwelling microwave radiances, it cannot, unfortunately, be easily characterized in terms of a single unknown variable. Observed cloud structures, however, may be utilized to overcome this problem. The AMSR-E algorithm uses output from a radar/radiometer algorithm developed for the TRMM sensor to prescribed cloud structures. The method is described in Kummerow et al. (2010), but essentially constructs cloud vertical structures at the 4 km PR resolution that are physically consistent with both radar and radiometer observations. These hydrometeors are then used as input to radiative transfer computations at AMSR-E frequencies and view angles, and the brightness temperature field is then convolved with the approximate AMSR-E antenna gain function to produce a large set of possible cloud profiles along with their respective passive microwave brightness temperatures. The main advantage of convolving the high-resolution brightness temperatures is that rainfalls in homogeneities are naturally represented in the method. Having statistically verified the cloud model in homogeneity against ground-based radar results, there is thus no further need to make corrections for inhomogeneous rainfall.

Databases are generated separately for different Sea Surface Temperature and Water vapor states. Sea Surface temperature is obtained from Reynolds (2002) SST climatology while the Total Precipitable Water (TPW) is computed internally to be consistent with the TPW in the a-priori database.

Once a database of profiles and associated brightness temperatures is established, the retrieval employs a straightforward Bayesian inversion methodology. In this approach, the probability of a particular profile R, given Tb can be written as:

$$Pr(R \mid Tb) = Pr(R) \times Pr(Tb \mid R) \quad (3)$$

where Pr(R) is the probability that a certain profile R will be observed and Pr(TB | R) is the probability of observing the brightness temperature vector, **TB**, given a particular rain profile R. The first term on the right hand side of Eq. 3 is derived using the GCE model information. The second term on the right hand side of Eq. 3, is obtained from radiative transfer computations through the cloud model profiles. The formal solution to the above problem is presented in detail in Kummerow et al. (1996), as well as Wilheit et al. (2003).

Instantaneous Land Rainfall

Rainfall retrievals over land are far more difficult than oceanic retrievals due to the large and variable emissivity of the land surface. Specifically, the high emissivity masks the emission signature that is related directly to the water content in the atmosphere. Instead, only the brightness temperature depression due to scattering in the upper portion of clouds is observed. The scattering, as shown in Fig. 2, increases with increasing frequencies. Consequently, brightness temperature depressions at the 89-GHz channel of AMSR-E will contain the least ambiguous signal of scattering by ice and/or large raindrops.

A further complication that arises over land is the lack of consistent backgrounds against which to compare the TB depression. To alleviate this problem caused by the varying emissivity associated with changes in surface characteristics (e.g., surface wetness, snow cover, vegetation, etc.), a rain/no-rain temperature depression threshold is required. Additionally, snow and desert surfaces cause depressed TBs at high frequencies (due to surface volume scattering) and can be confused with the rain signature. If these surface types are not properly screened, they can be misinterpreted as ice scattering in clouds.

The original basis for the retrieval over land comes from the work of Grody (1991), who developed a global scattering index (SI) at 85 GHz for use with the SSM/I sensor. Further refinement of the technique is described in Ferraro et al. (1994), Ferraro (1997), and Li et al. (1998). The rationale was to first develop a relationship that could best predict the 85-GHz TB under "non-scattering" conditions for the land surface in question. Then, by estimating this value and subtracting the actual 85-GHz TB, a measure of the depression due to scattering by precipitation ice/rain drops could be determined. Scattering Index (SI) values in excess of 10 K were found to be a good global indicator of rain. Later it was found that a simple difference between TB 22 V and TB 85 V yielded similar results, and it forms the basis for the current AMSR-E rain over land algorithm. Specifically, the land portion of the algorithm begins with a Scattering Index (SI):

$$SI = 451.9 - 0.44 \bullet Tb_{19V} - 1.775 \bullet Tb_{22V} + 0.00575 \bullet Tb^2_{22V} - Tb_{85V} \quad (4)$$

When using the SI-type approach over land, it is critical that similar scattering signatures caused by other surfaces such as snow cover, desert sand and semi-arid regions be filtered to avoid false signatures (Grody 1991). SI values greater than 10 K identify rain areas, and subsequent screens remove snow-covered, desert, and semi-arid land regions.

McCollum et al. (1999) used SSM/I data to optimize two screening methodologies described in Li et al. (1998) and to evaluate both methods to document and improve their deficiencies. The two methodologies are the NESDIS screening of Ferraro (1997) and the GSCAT2 screening used in the early versions of GPROF over land, algorithm, and at this writing, in TRMM TMI production algorithm (currently denoted TRMM V7; see Gopolan et al. 2010). In general, the NESDIS based screening tends to be more liberal in nature and allows for rain identification in colder environments (at the expense of misclassification due to melting snow) while GPROF is more conservative and flags these areas as indeterminate (at the expense of eliminating moderate to heavy rainfall in winter seasons). GPROF also appears to suffer from some inadequate screening in semi-arid areas. McCollum et al. (1999) developed a methodology that adopts the more conservative GPROF approach but uses spatial information from neighboring pixels to “fill-in” indeterminate areas. An additional modification to previous rain/no-rain temperature depression thresholds was made.

To depart from the scattering index (Eq. B4) SI 10-K threshold, which was determined specifically for SSM/I data, a more generic difference between low and high frequency SSM/I channels is used. A 22 V – 85 V threshold of 8 K was found to be appropriate for identification of pixels with rain.

Because of the non-uniqueness in resolving proper hydrometeor profiles, the use of physical retrieval algorithms over land has been limited. Although the proper surface rain rates may be retrieved by matching the observed TBs to model simulations, the intervening atmospheric cloud constituents are typically incorrect due to the lack of information available from the SSM/I. An alternative method to retrieve rain rate has been to calibrate the SI with ground-based radar measurements from the United States, Japan, and the United Kingdom (Ferraro and Marks, 1995). They found that a scaled, nearly squared value of SI correlated well with rain rate. Specifically, the following relationship was found to work best for global applications:

$$RR(mm/hr) = 0.00513 \bullet SI^{1.9468} \tag{4}$$

where *RR* is in mm/hr. Since these relationships increase rapidly for higher values of SI, any retrieval above 35 mm/hr is set to 35 mm/hr. Although somewhat arbitrary, practice shows that this is the upward limit of rain rates retrievable from the 85-GHz measurements (e.g., the maximum mean rain rate that could exist in a 13 by 15 km FOV). Using the 10 K minimum threshold for the SI values, the minimum retrievable rain rate is approximately 0.5 mm/hr. This algorithm was implemented by FNMOC in 1995 as the operational SSM/I rain rate algorithm (i.e., available in the EDR files for SSM/I), and continues to operate in that capacity. In addition, the monthly derived rainfall from this algorithm (Ferraro 1997) is used as a component of the GPCP blended analysis (Huffman et al. 1996), is continually updated, is archived at the National Climatic Data Center (http://www.ncdc.noaa.gov/ol/satellite/ssmi/ssmiproducts.html).

The AMSR instrument contains slightly different frequencies than the SSM/I (e.g., 89.0 instead of 85.5 GHz), contains more information (e.g., 10 channels vs. 7), and also has

significantly higher spatial resolution. It is therefore convenient to have a physical basis for modifying SSM/I algorithms to suit the AMSR observations. To accomplish this, as well as to simplify the retrieval process, the AMSR precipitation team decided to use the same GPROF retrieval methodology as used for the ocean retrieval (Wilheit et al. 2003). Unlike the ocean component, however, the initial database of possible profiles was carefully selected to include only those profiles that fit the empirical relation developed by Ferraro and Marks (1995), given in Eq. (B5). The relationship of Eq. (B5) was reproduced by selecting 36 profiles fitting Eq. (B5) out of the several thousand profiles in the GPROF database. The expected AMSR-E TBs were then computed for these profiles for use in the *a-priori* look-up-table used in the algorithm.

After Aqua launch and through other investigations focused on the GPROF versions for SSM/I and TMI, it was found that the original relationship between SI and rain rate was biased, in particular, over convective areas, where the rain rate was too high (McCollum et al. 2002). To improve the Bayesian scheme by providing more realistic relationships between surface rain rate and 85-GHz temperature depressions, matchups between the TRMM PR and TMI were assembled (McCollum and Ferraro 2003). It was learned that improved rain rates could be obtained by having both convective and stratiform relationships between Tb 85 V and rain rate, and having those profiles in the GPROF database be restricted to these relationships. The final rain rate is then computed via a probability of convective index (based on a regression relationship that utilizes several channel measurements), then taking a weighted average of the convective and stratiform rain rates that corresponds to profile matches of the Tb at 85 V. More details on the algorithm are summarized in McCollum and Ferraro (2003).

More recently, after many more years of evaluation, in particular, between TRMM TMI and PR, it was found that a substantial warm season bias existed with this algorithm (Wang et al. 2009). Subsequently, through the use of 8 years of TMI and PR matchups, both an imroved set of CI coefficients and TB to RR relationships were developed (Gopolan et al. 2010) and have successfully been incorporated for use with AMSR-E.

References

Chandrasekhar, S. 1960. *Radiative Transfer*. New York: Dover Publications.

Ferraro, R. R. 1997. SSM/I derived global rainfall estimates for climatological applications. *J. of Geophys. Res.* 102: 16,715-16,735.

Ferraro, R. R. and G. F. Marks. 1995. The development of SSM/I rain rate retrieval algorithms using ground based radar measurements. *J. Atmos. Oceanic Tech*. 12: 755-770.

Ferraro, R. R., N. C. Grody, and G. F. Marks. 1994. Effects of surface conditions on rain identification using the SSM/I. *Rem. Sens. Rev*. 11: 195-209.

Gopolan, K., N. Y. Wang, C. Liu, and R. Ferraro**.** 2010. Version 7 of the TRMM 2A12 Land Precipitation Algorithm. *J. Atmos. Oceanic Tech.* 27: 1343-1354.

Grody, N. C. 1991. Classification of snow cover and precipitation using the Special Sensor Microwave/Imager (SSM/I). *J. of Geophys. Res*. 96: 7423-7435 .

Huffman, G. J., R. F. Adler, P. Arkin, A. Chang, R. Ferraro, A. Gruber, J. Janowiak, A. McNab, B. Rudolf, and U. Schneider. 1996. The global precipitation climatology project (GPCP) combined precipitation data set. *Bull. Amer. Meteor. Soc*. 78: 5-20.

Kummerow, C., W. S. Olson, and L. Giglio. 1996. A Simplified Scheme for Obtaining Precipitation and Vertical Hydrometeor Profiles from Passive Microwave Sensors. *IEEE Trans. on Geosci. and Rem. Sen*. 34: 1213-1232.

Kummerow, C. D., S. Ringerud, J. Crook, D. Randel, and W. Berg. 2010: An observationally generated *A-Priori* database for microwave rainfall retrievals. *J. Atmos. and Oceanic Tech*. 28(2): 113-130.

Li, Q., R. Ferraro, and N. C. Grody. 1998. Detailed analysis of the error associated with the rainfall retrieved by the NOAA/NESDIS SSM/I Rainfall Algorithm: Part I. Tropical oceanic rainfall. *J. Geophys. Res*. 103: 11,419-11,427.

McCollum, J. R. and R. R. Ferraro. 2003. The next generation of NOAA/NESDIS SSM/I, TMI and AMSR-E microwave land rainfall algorithms. *J. Geophys. Res.* 108**:** 8382-8404.

McCollum, J. R. and R. R. Ferraro. 2005. Microwave Rainfall Estimation along coasts. *J. Atmos. Ocean. Technol.* 22: 497-512.

McCollum, J. R., A. Gruber, and M. B. Ba. 1999. Discrepancy between gauges and satellite estimates of rainfall in equatorial Africa. *J. Appl. Meteor*. 41: 1065-1080.

McCollum, J., W. Krajewski, R. Ferraro and M. Ba. 2002. Evaluation of biases of Satellite Rainfall Estimation algorithms over the continental U.S. *J. Appl. Meteor.* 41: 1065 –1080.

Reynolds, R. W., N. A. Rayner, T. M. Smith, D. C. Stokes, and W. Wang. 2002. An improved in situ and satellite SST analysis for climate. *J. Climate* 15: 1609–1625.

Tao, W. -K. and J. Simpson. 1993. Goddard Cumulus Ensemble model, Part I: Model description. *TAO* 4: 35-72.

Tripoli, G. J. 1992. An explicit three-dimensional nonhydrostatic numerical simulation of a tropical cyclone. *Meteorol. Atmos. Phys*. 49: 229-254.

Wang, N., C. Liu, R. Ferraro, D. Wolff, E. Zipser, and C. Kummerow. 2009. The TRMM 2A12 Land Precipitation Product – Status and Future Plans. *J. of Meteor. Soc. Of Japan* 87: 237 – 253.

Wilheit, T. T., A. T. C. Chang, M. S. V. Rao, E. B. Rodgers, and J. S. Theon. 1977. A satellite technique for quantitatively mapping rainfall rates over the ocean. *J. Appl. Meteor.* 16: 551-560.

Wilheit, T. T., A. T. C. Chang, and L. S. Chiu. 1991. Retrieval of monthly rainfall indices from microwave radiometric measurement using probability distribution functions. *J. Atmos. Oceanic. Technol.* 8: 118-136.

Wiheit, T., C. Kummerow, and R. Ferraro. 2003. Rainfall algorithms for AMSR-E. *IEEE Trans. Geosci. and Rem.Sens.* 41: 204-214.